NANO LETTERS

Letter

pubs.acs.org/NanoLett

Electronic and Transport Properties of Unbalanced Sublattice N-Doping in Graphene

Aurélien Lherbier,* Andrés Rafael Botello-Méndez, and Jean-Christophe Charlier

Institute of Condensed Matter and Nanosciences (IMCN), Université catholique de Louvain (UCL), 1348 Louvain-la-Neuve, Belgium

ABSTRACT: Using both first-principles techniques and a real-space Kubo-Greenwood approach, electronic and transport properties of nitrogen-doped graphene with a single sublattice preference are investigated. Such a breaking of the sublattice symmetry leads to the appearance of a true band gap in graphene electronic spectrum even for a random distribution of the N dopants. More surprisingly, a natural spatial separation of both types of charge carriers at the band edge is predicted, leading to a highly asymmetric electronic transport. Both the presence of a band gap, allowing large on/off ratio, and an asymmetric transport pave a new route toward efficient graphene-based field-effect transistors.

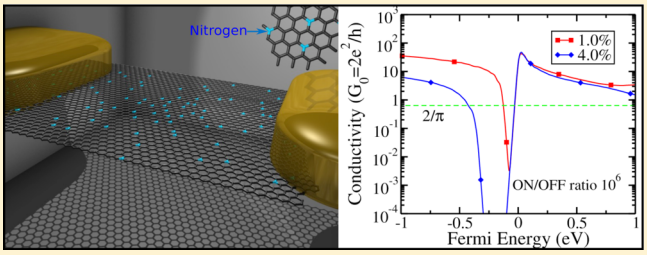

KEYWORDS: *Graphene FET, electronic transport, nitrogen doping, band gap, ab initio, tight-binding*

Early transport measurements of graphene, a one-atom thick layer of carbon with outstanding properties and promising applications,[1−4] revealed extremely high carrier mobilities.[5] This placed graphene at the spotlight for future field-effect transistors (FETs). Indeed, the new fundamental physics due to the massless Dirac fermions in graphene[6] will probably lead to new emergent applications for future nanoelectronics.[7] However, graphene is a zero overlap semimetal and the absence of a true band gap is a major drawback to achieve high I_{on}/I_{off} ratio as required for FETs. Therefore, it was realized quite early that pristine graphene will not likely replace silicon in digital transistors as used in the current complementary metal-oxide-semiconductor (CMOS) technology. Notwithstanding, an alternative for graphene-based FET (G-FET) consisting in a new type of vertical transistor architecture has been proposed.[8] Prior to the vertical FET approach, several theoretical and experimental works have investigated various possibilities to open a gap in graphene.[9]

One route to open a band gap in a material consists in a dimensional narrowing. The resulting electronic confinement increases energy separation between eigenstates. Cutting graphene into quasi-1D ribbons may be a good strategy,[10] providing that the channel width reduction does not lead to a detrimental increase of scattering such as edge imperfections.[11] A second way to obtain a band gap is to fully functionalize graphene with, for instance, hydrogen (graphane[12]) or fluor (fluorographene[13]). However, the change of hybridization into sp^3 carbon atoms degrade the transport properties compared to sp^2 graphene systems. Another approach focused on transport gaps generated by localization phenomena.[14,15] For that purpose, the disorder potential has to exhibit preferentially a strong short-range contribution to allow intervalley backscattering since direct intravalley backscattering is normally forbidden by pseudospin symmetry. In case of strongly (structurally or chemically) disordered graphene systems, an Anderson insulator behavior can indeed be observed.[16,17] Finally, superlattices of dopants,[18] adsorbates, or patterned holes,[19] have also been proposed as an alternative to open a band gap in graphene.

In this Letter, the transport properties of graphene doped with nitrogen (N), preferentially distributed in one of the two triangular sublattices of the honeycomb lattice, are studied. This theoretical work is motivated by recent experimental synthesis of N-doped graphene samples whose atomistic characterizations have evidenced such unbalanced sublattice doping.[20,21] For this particular doping configuration, the system exhibits striking phenomena which are particularly interesting for G-FETs applications but presumably also for graphene-based optoelectronics. Indeed, the single sublattice doping does not only open a sizable true band gap but also leads to a natural spatial separation of carriers being at the origin of a quasi-ballistic transport behavior at the conduction band edge. This unconventional effect is deeply linked to the bipartite nature of the honeycomb lattice and the corresponding symmetry of the electronic wave function.[22]

Ab initio Electronic Structure. First-principles simulations have been conducted using the SIESTA package[23] in the generalized gradient approximation for the exchange-correlation functional in the Perdew−Burke−Ernzerhof (PBE) form[24] with the PBEsol parametrization.[25] Troullier-Martins pseudopotentials are used to account for the core electrons.[26] The valence electron wave functions are expanded in a double-ζ polarized basis set of finite-range numerical pseudoatomic

Received: November 26, 2012
Revised: February 19, 2013
Published: March 11, 2013

   dx.doi.org/10.1021/nl304351z | *Nano Lett.* 2013, 13, 1446−1450

orbitals.[27] The system consists in a 10 × 10 graphene supercell containing 200 atoms including a single substitutional N dopant seating in one of the two sublattices. The supercell technique implies periodic repetitions of the cell. Thus, the system can be considered as an infinite graphene sheet with a superlattice of N atoms in sublattice A, inducing an n-type doping concentration x_N = 1/200 = 0.5%.

The corresponding ab initio band structure and density of states (DOS) are presented in Figure 1 (thick black lines). The

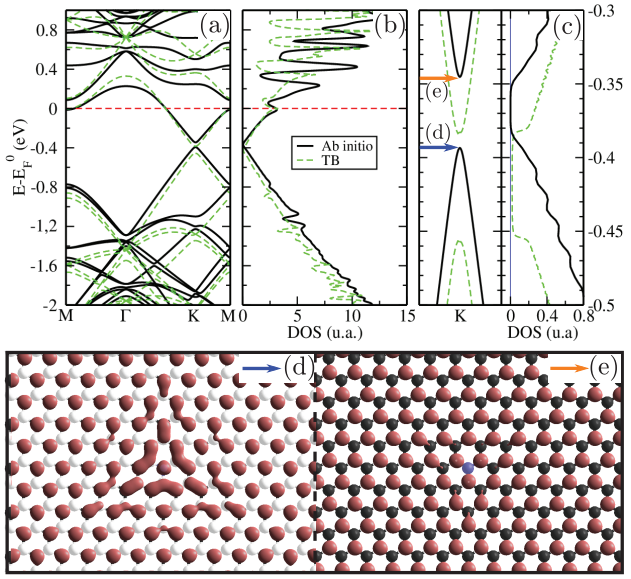

Figure 1. Ab initio (thick black lines) and tight-binding (green dashed lines) band structures (a) and DOS (b) of a 10 × 10 graphene supercell containing one substitutional N dopant. (c) Zoom of band structure (left panel) and DOS (right panel) close to the band gap. Isosurfaces of the wave function at the K point just below (d) and above (e) the band gap (blue/orange arrows in panel (c)). The N atom is colored in blue, while C atoms in A/B sublattice are colored in black/white, respectively.

zero energy is aligned with the equilibrium Fermi energy (E_F^0) (horizontal dashed red line) lying at the half-filled first π^* conduction band. When only one sublattice is modified, a band gap (here E_g = 50 meV) is generated at the former Dirac points (K/K'). Such band gap opening due to a superlattice of dopants has already been discussed in ref 18.

In addition to the band gap opening, our calculations predict a modification of the electronic wave function of the charge carriers at the band gap edges. In pristine graphene, the wave function around a given K point is defined with equivalent weights in both A and B sublattices, differing only by a complex phase.[28] This specific symmetry gives rise to the pseudospin degree of freedom. When only one of the two sublattices is perturbed, such a symmetry is broken, thus modifying the charge carrier spatial distribution. In such a case, the wave function at the K (as well as at K') point, corresponding to carriers at the band edges, is mainly located in only one sublattice (Figure 1d,e). Carriers below the band gap, that is, holes, live in sublattice A containing the N atom (only the white C atoms of sublattice B are visible in Figure 1.d). In contrast, above the band gap, electrons live in sublattice B (only the black C atoms of sublattice A are visible in Figure 1e). Such a charge carrier separation on both sublattices is not an artifact of image interactions which could appear in too small supercell.[29] Calculations on a larger supercell (4000 C atoms) with a distance between the N atom and its images >100 Å confirmed that those band edge states are indeed extended states.

Tight-Binding Model. An orthogonal third nearest-neighbors $\pi-\pi^*$ tight-binding (TB) model is used to describe the electronic structure of large graphene sheets (250 × 250 nm^2) containing ∼2.4 millions of atoms. The TB parameters of this model[16] are composed of a single on-site term ε_{p_z} = 0.59745 eV and three hopping terms γ_0^1 = −3.09330 eV, γ_0^2 = 0.19915 eV, γ_0^3 = −0.16214 eV corresponding to first, second, and third nearest neighbors, respectively. The TB parametrization of the substitutional N atom has been performed by fitting the ab initio band structure described previously.[30] The TB band structure and DOS are presented in Figure 1 (green dashed lines) and compared to the ab initio results. The apparent down shift of the TB valence band structure can be explained as follows. The TB model used for pristine graphene yields to a good agreement with ab initio results especially for the valence band. The description of the conduction band in the K−M branch is less accurate leading to a shift of the van Hove singularity and corresponding conduction bands to higher energies.[16] In Figure 1a,b, since the band structure is aligned to the Fermi energy lying in the first π^* conduction band, all the π-valence bands thus appear slightly shifted to lower energies.

Large graphene planes containing various concentrations of N dopants randomly distributed in one sublattice are investigated using this TB model. The corresponding DOS are depicted in Figure 2. Note that the band gap induced by

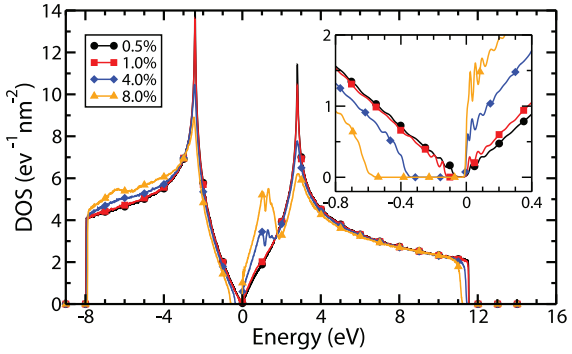

Figure 2. Density of states of graphene containing various concentrations of N dopants randomly distributed in one sublattice. Inset: Zoom of DOS in the band gap region.

sublattice asymmetry is robust with respect to such a random distribution of N dopants in one sublattice. Its amplitude ranges from E_g = [45;110;340;550] meV for various N concentration corresponding to x_N = [0.5;1;4;8]% (inset of Figure 2).[31] The band gap dependence with the N concentration scales as $E_g(x_N) \propto x_N^{0.75}$. Similar band gap opening for vacancies randomly distributed in the same sublattice was obtained by Pereira et al.,[32] although in that case a zero energy mode persists inside the gap.

Transport Methodology. The transport properties are computed from the dynamics of electronic wavepackets with an order-N Kubo-Greenwood method described in details in refs 16 and 33. To summarize, the dynamics is monitored through the time-dependent diffusivity coefficient $D(E,t) = \Delta R^2(E,t)/t$, with E the energy of the carriers, $\Delta R^2 = \Delta X^2 + \Delta Y^2$, and

dx.doi.org/10.1021/nl304351z | Nano Lett. 2013, 13, 1446−1450

$\Delta X^2(E,t) = \mathrm{Tr}[\delta(E-\hat{H})|\hat{X}(t)-\hat{X}(0)|^2]/\mathrm{Tr}[\delta(E-\hat{H})]$ the quadratic spreading along the x direction. Tr is the trace over p_z orbitals and $\mathrm{Tr}[\delta(E-\hat{H})]/S = \rho(E)$ is the total DOS (per unit of surface S). The results are averaged over multiple initial random phase wavepackets. The transport properties are inferred from the time evolution of $D(E,t)$. At very short times, the wavepacket dynamics is quasi-ballistic, so that $D(E,t) \sim v^2(E)t$, where $v(E)$ is the carrier velocity. The dynamics further becomes diffusive as the carriers get scattered by the disorder, and $D(E,t)$ reaches a maximum value $D_{max}(E) = 2v(E)l_e(E)$, where $l_e(E)$ is the mean free path. The semiclassical conductivity then reads $\sigma_{sc}(E) = (1/4)e^2\rho(E)D_{max}(E)$. All the simulations are conducted at 0 K meaning that the electronic transport is coherent. Therefore, at longer propagation times weak localization corrections due to multiple scattering events per carrier can cause $D(E,t)$ to decrease.

Diffusivity, Mean Free Path, Conductivity, and Mobility. The diffusivity coefficient ($D(E,t)$) at specific energies is presented in (Figure 3a,b). For an energy sufficiently close to the conduction band edge (E = 0.01 eV) a quasi-ballistic regime is observed. Indeed, $D(t)$ presents an unsaturated behavior meaning that the steady state of the diffusive regime is not yet reached. This behavior is a clear signature of a very low scattered electronic transport.[34] Indeed, according to the wave function distribution (Figure 1e), the electrons live mainly in the sublattice that does not contain the N atoms. For those carriers, the scattering process with the N atoms is rather inefficient, thus giving rise to a quasi-ballistic transport regime. Note that this quasi-ballistic behavior turns rapidly to a quasi-diffusive regime with an almost saturated diffusivity coefficient as observed at E = 0.05 eV. Since the diffusive regime is not completely reached at the conduction band edge, semiclassical transport quantities such as l_e, σ_{sc}, and μ cannot be in principle defined. However in Figure 3c–e, transport quantities at the conduction band edge have been extracted using the highest $D(E,t)$ value and are given as an indication. This means that l_e, σ_{sc}, and μ values at the conduction band edge should actually be even higher. Finally, localization effects are predicted for energies around the N resonant energy ($E \sim 1$ eV)[35] as confirmed by the decrease of the diffusivity coefficient ($D(E,t)$) at a very early propagation time.

The computed mean free path, plotted in logarithmic scale in Figure 3c, exhibits an interesting asymmetric behavior depending on the nature of charge carriers. For holes, l_e decreases slowly with decreasing carrier energy and is even constant (~5 nm) in case of high N concentration (4%). Inside the band gap, l_e is undefined (shaded regions in Figure 3). For electrons, a strong divergence of l_e is observed at the band gap edge with corresponding values of few hundreds of nanometers. Then, for increasing carrier energies, a rapid decrease of l_e down to few nanometers is predicted with a minimum at $E \sim 1$ eV, which corresponds to the dopant resonant energy revealed by a peak in the DOS at the same energy (see Figure 2).

Identically to l_e, σ_{sc} is undefined inside the band gap and is thus set to zero. The effect of a smearing Fermi–Dirac temperature (T) can be accounted for by expressing $\sigma_{sc}(E_F,T) = -\int_{-\infty}^{+\infty} dE'((\partial f(E_F,E',T))/\partial E')\sigma_{sc}(E',0\ \mathrm{K})$, where $f(E_F,E,T)$ is the Fermi–Dirac distribution function and E_F is the corresponding Fermi energy. In a FET device, the position of the Fermi level (E_F) can be displaced from its equilibrium position (E_F^0) by applying a gate voltage (V_g). The semiclassical

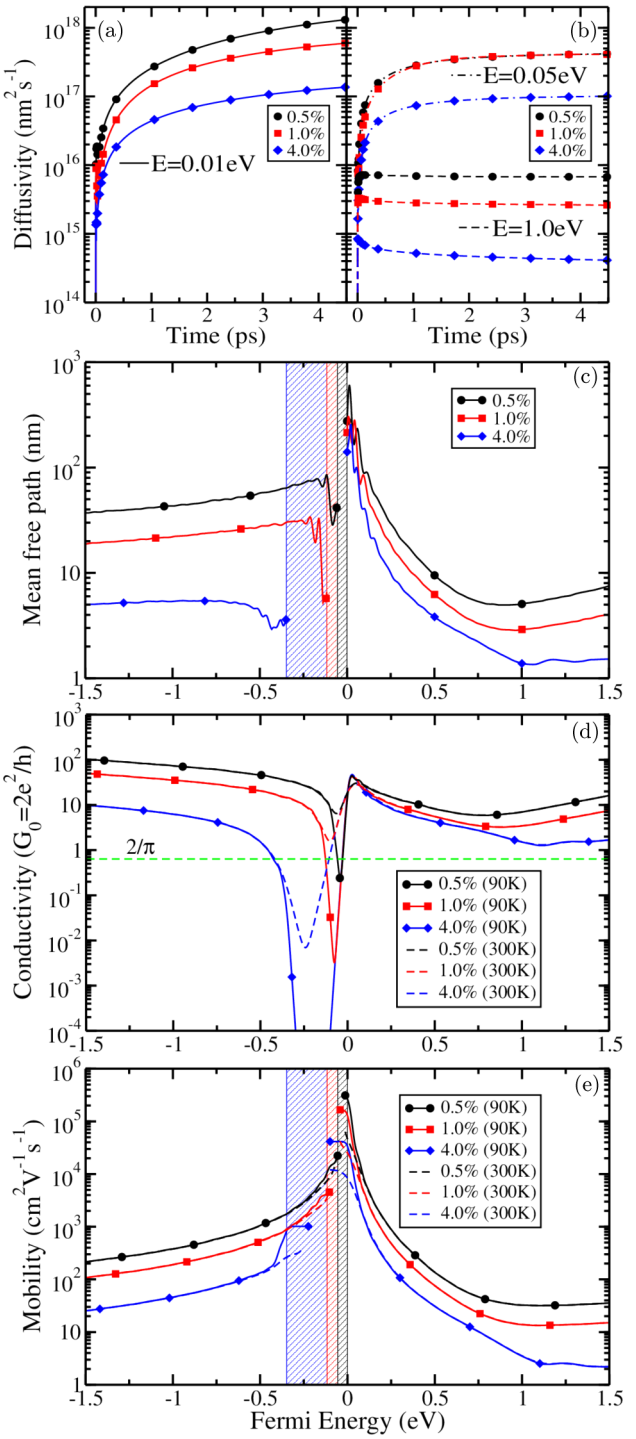

Figure 3. Transport properties in graphene for various concentrations of N dopants randomly distributed in one sublattice. (a,b) Diffusivity versus time at three different energies, (a) E = 0.01 eV (thick lines), (b) E = 0.05 eV (dashed-dotted lines) and E = 1.0 eV (dashed lines), (c) carrier mean free paths, (d) semiclassical conductivities, and (e) mobilities. The shaded regions indicate the corresponding band gap energy windows.

conductivities for Fermi–Dirac temperatures T = 90 K and T = 300 K are presented in Figure 3d. The well-known lower limit of the semiclassical conductivity ($\sigma_{sc}^{min} = (2/\pi)G_0 = [(4e^2)/(\pi h)]$) for gapless graphene is also indicated as a horizontal dashed green line. For $T > 0$ K, $\sigma_{sc}(T)$ can be evaluated near the band edge, inside the band gap, which tends to shorten the

dx.doi.org/10.1021/nl304351z | Nano Lett. 2013, 13, 1446–1450

conductivity gap and eventually close it if the band gap is too small. For x_N = 0.5%, the band gap being rather small (45 meV), the minimal value of $\sigma_{sc}(T = 90\ K)$ is just below σ_{sc}^{min} meaning that the presence of the band gap is hidden and that low temperatures are required to clearly observe it. For x_N = 4%, the band gap being wider (340 meV), σ_{sc} goes largely below σ_{sc}^{min} even at T = 300 K. Just above the band gap, σ_{sc} increases sharply to a value of ∼50 G_0. This is 2 orders of magnitudes higher than in the band gap for x_N = 0.5% at T = 90 K. For higher x_N, the ratio between on and off state increases rapidly up to 10^4−10^6. Interestingly, if the hole conductivity remarkably decreases with increasing N concentration the electron conductivity at the band edge is maintained to high values. This is explained by the quasi-ballistic transport occurring at this band edge.

The charge carriers mobility (μ), illustrated in Figure 3e, can be evaluated with the conductivity and the computation of the charge carrier density (n) as, $\mu(E_F,T) = (\sigma_{sc}(E_F,T))/(en(E_F,T))$, where e is the elementary charge. Since by definition μ is inversely proportional to n, a natural divergence of the mobility can be obtained when n vanishes, provided that σ_{sc} does not vanish accordingly. In pristine graphene, this condition is realized since σ_{sc} possesses a finite limit value (σ_{sc}^{min}), which partly explains the extremely high mobilities measured in clean graphene. The location of the Fermi level at equilibrium (E_F^0, that is, at V_g = 0), which determines the separation between holes and electrons carriers (i.e., the charge neutrality point), is of great importance to maximize the mobility. E_F^0 can be modulated by choosing the proper work function of the electrodes or by changing the substrate for instance. In the present single-sublattice N-doped graphene system, E_F^0 is naturally positioned above the band gap (see Figure 1). To maximize the mobility, E_F^0 has to be pinched to conduction band edge, or inside the gap. Here, we assume that such ideal conditions can be realized and that E_F^0 lies in the gap. Electron (respectively hole) carrier density is thus defined as $n_{elec}(E_F,T) = \int_{E_F^0}^{+\infty} dE' f(E_F,E',T)\rho(E')$, $n_{hole}(E_F,T) = \int_{-\infty}^{E_F^0} dE' (1-f(E_F,E',T))\rho(E')$. Even if the DOS, and thus n, increases quite fast at the conduction band edge, good mobilities (>10^4 cm^2 V^{-1} s^{-1}) are still obtained, even for x_N as high as 4%. The appearance of a small plateau of constant mobility in the vicinity of the band edge is explained by the fact that in this energy region, σ_{sc} is linearly proportional to n. A variation of more than 1 order of magnitude is observed between electron and hole mobilities. The reported asymmetrical behaviors of l_e, σ_{sc}, and μ, in concordance with the presence of the band gap are highly desirable for conventional logic devices.

Discussion. The largest band gap opening obtained for the case of a perfectly unbalanced sublattice doping (∼550 meV for x_N = 8%) exceeds the minimum required band gap for high-speed CMOS (340 meV).[36] Similar N concentrations but with distribution of 80% in sublattice A and 20% in sublattice B have also been investigated. A true band gap persists although reduced as a result of the loss of asymmetry between the two sublattices. Note that the TB band gaps are derived from TB parameters fitted to reproduce density functional theory (DFT) calculations. However, DFT is known to systematically underestimate band gaps compared to experimental values. Consequently, real band gaps in unbalanced sublattice doped graphene are expected to be larger than the present underestimated TB predictions. A strategy to obtain larger gaps would consist in increasing sublattice asymmetry by codoping the graphene sheet with N in one sublattice and boron (B) in the other sublattice.[37] However, this will also introduce scattering centers in both sublattices destroying the quasi-ballistic transport regime discussed above. Moreover, such selective sublattice B/N codoping is probably difficult to achieve experimentally without forming BN domains.[38] The existence of a natural electron−hole spatial separation around the obtained gap, could be relevant for optoelectronics. In particular, a photoexcited electron−hole pair should exhibit an inefficient recombination due to the small overlap between the electron and hole wave functions. However, more accurate investigations are needed to confirm these predictions well beyond the scope of the present research.

Conclusion. Electronic and transport properties of large graphene sheets doped with N substitutional atoms in only one sublattice have been investigated theoretically. The symmetry break of the bipartite graphene lattice leads to the appearance of a true band gap tunable with dopant concentrations. The band gap is found to be robust with respect to a random distribution of the N atoms in the sublattice. In addition, around the band gap a spatial separation of charge carriers in each sublattice is observed, offering an interesting feature for future graphene-based optoelectronics. Moreover, the carriers at the conduction band edge exhibit good transport properties with long mean free paths, high conductivities and mobilities. These electrons live mainly in the unaltered sublattice where low scattering rate occurs, resulting in a quasi-ballistic behavior. The presence of both a tunable band gap and the existence of carriers traveling in an unperturbed sublattice suggests the use of lattice-selective doped graphene in GFET applications. These findings encourage deeper theoretical transport investigations taking into account gate and dielectric environment,[39] as well as transport measurements on N-doped graphene samples where such an unbalanced sublattice doping has been observed.[20,21]

AUTHOR INFORMATION

Corresponding Author

*E-mail: aurelien.lherbier@uclouvain.be.

Notes

The authors declare no competing financial interest.

ACKNOWLEDGMENTS

J.-C.C., A.L., and A.R.B.-M. acknowledge financial support from FNRS of Belgium. This work is connected to the ARC Graphene Nanoelectromechanics (No. 11/16-037). Computational resources are provided by the UCL-CISM.

REFERENCES

(1) (a) Lee, B.-J.; Yu, H.-Y.; Jeong, G.-H. *Nanoscale Res Lett* **2010**, *5*, 1768−1773. (b) Khrapach, I.; Withers, F.; Bointon, T. H.; Polyushkin, D. K.; Barnes, W. L.; Russo, S.; Craciun, M. F. *Adv. Mater.* **2012**, *24* (21), 2844−2849.

(2) Bae, S.; Kim, H.; Lee, Y.; Xu, X.; Park, J.-S.; Zheng, Y.; Balakrishnan, J.; Lei, T.; Kim, H. R.; Song, Y. I.; Kim, Y.-J.; Kim, K. S.; Özyilmaz, B.; Ahn, J.-H.; Hong, B. H.; Iijima, S. *Nat. Nanotechnol.* **2010**, *5* (8), 574−578.

(3) Gomez De Arco, L.; Zhang, Y.; Schlenker, C. W.; Ryu, K.; Thompson, M. E.; Zhou, C. *ACS Nano* **2010**, *4* (5), 2865−2873.

(4) (a) Murali, R.; Brenner, K.; Yinxiao, Y.; Beck, T.; Meindl, J. D. *IEEE Electron Device Lett.* **2009**, *30* (6), 611−613. (b) Xiangyu, C.; Akinwande, D.; Lee, K.-J.; Close, G. F.; Yasuda, S.; Paul, C. B.; Fujita, S.; Kong, J.; Wong, H.-S. P. *IEEE Trans. Electron Devices* **2010**, *57* (11), 3137−3143.

(5) Chen, J. H.; Jang, C.; Xiao, S.; Ishigami, M.; Fuhrer, M. S. *Nat. Nanotechnol.* **2008**, *3* (4), 206−209.
(6) Novoselov, K. S.; Geim, A. K.; Morozov, S. V.; Jiang, D.; Katsnelson, M. I.; Grigorieva, I. V.; Dubonos, S. V.; Firsov, A. A. *Nature* **2005**, *438* (7065), 197−200.
(7) (a) Novoselov, K. S. *Rev Mod Phys* **2011**, *83* (3), 837−849. (b) Novoselov, K. S.; Fal'ko, V. I.; Colombo, L.; Gellert, P. R.; Schwab, M. G.; Kim, K. *Nature* **2012**, *490* (7419), 192−200.
(8) Britnell, L.; Gorbachev, R. V.; Jalil, R.; Belle, B. D.; Schedin, F.; Mishchenko, A.; Georgiou, T.; Katsnelson, M. I.; Eaves, L.; Morozov, S. V.; Peres, N. M. R.; Leist, J.; Geim, A. K.; Novoselov, K. S.; Ponomarenko, L. A. *Science* **2012**, *335* (6071), 947−950.
(9) Schwierz, F. *Nat. Nanotechnol.* **2010**, *5* (7), 487−496.
(10) Tapasztó, L.; Dobrik, G.; Lambin, P.; Biró, L. P. *Nat. Nanotechnol.* **2008**, *3* (7), 397−401.
(11) (a) Areshkin, D. A.; Gunlycke, D.; White, C. T. *Nano Lett.* **2007**, *7* (1), 204−210. (b) Nakada, K.; Fujita, M.; Dresselhaus, G.; Dresselhaus, M. S. *Phys. Rev. B* **1996**, *54* (24), 17954−17961.
(12) Elias, D. C.; Nair, R. R.; Mohiuddin, T. M. G.; Morozov, S. V.; Blake, P.; Halsall, M. P.; Ferrari, A. C.; Boukhvalov, D. W.; Katsnelson, M. I.; Geim, A. K.; Novoselov, K. S. *Science* **2009**, *323* (5914), 610−613.
(13) Nair, R. R.; Ren, W.; Jalil, R.; Riaz, I.; Kravets, V. G.; Britnell, L.; Blake, P.; Schedin, F.; Mayorov, A. S.; Yuan, S.; Katsnelson, M. I.; Cheng, H.-M.; Strupinski, W.; Bulusheva, L. G.; Okotrub, A. V.; Grigorieva, I. V.; Grigorenko, A. N.; Novoselov, K. S.; Geim, A. K. *Small* **2010**, *6* (24), 2877−2884.
(14) Lagendijk, A.; van Tiggelen, B.; Wiersma, D. S. *Phys. Today* **2009**, *62* (8), 24−29.
(15) (a) Biel, B.; Triozon, F.; Blase, X.; Roche, S. *Nano Lett.* **2009**, *9* (7), 2725−2729. (b) Cresti, A.; Lopez-Bezanilla, A.; Ordejón, P.; Roche, S. *ACS Nano* **2011**, *5* (11), 9271−9277.
(16) (a) Lherbier, A.; Dubois, S. M.-M.; Declerck, X.; Roche, S.; Niquet, Y. M.; Charlier, J.-C. *Phys. Rev. Lett.* **2011**, *106* (4), 046803−046806. (b) Lherbier, A.; Dubois, S. M.-M.; Declerck, X.; Roche, S.; Niquet, Y. M.; Charlier, J.-C. *Phys. Rev. B* **2012**, *86* (7), 075402−075419.
(17) Leconte, N.; Moser, J.; Ordejon, P.; Tao, H.; Lherbier, A.; Bachtold, A.; Alsina, F.; Sotomayor, C. M.; Charlier, J.-C.; Roche, S. *ACS Nano* **2010**, *4* (7), 4033−4038.
(18) (a) Martinazzo, R.; Casolo, S.; Tantardini, G. F. *Phys. Rev. B* **2010**, *81* (24), 245420−245427. (b) Casolo, S.; Martinazzo, R.; Tantardini, G. F. *J. Phys. Chem. C* **2011**, *115* (8), 3250−3256.
(19) Pedersen, T. G.; Flindt, C.; Pedersen, J.; Mortensen, N. A.; Jauho, A.-P.; Pedersen, K. *Phys. Rev. Lett.* **2008**, *100* (13), 136804−136807.
(20) Zhao, L.; He, R.; Rim, K. T.; Schiros, T.; Kim, K. S.; Zhou, H.; Gutiérrez, C.; Chockalingam, S. P.; Arguello, C. J.; Pálová, L.; Nordlund, D.; Hybertsen, M. S.; Reichman, D. R.; Heinz, T. F.; Kim, P.; Pinczuk, A.; Flynn, G. W.; Pasupathy, A. N. *Science* **2011**, *333* (6045), 999−1003.
(21) Lv, R.; Li, Q.; Botello-Méndez, A. R.; Hayashi, T.; Wang, B.; Berkdemir, A.; Hao, Q.; Elías, A. L.; Cruz-Silva, R.; Gutiérrez, H. R.; Kim, Y. A.; Muramatsu, H.; Zhu, J.; Endo, M.; Terrones, H.; Charlier, J.-C.; Pan, M.; Terrones, M. *Nat. Sci. Rep.* **2012**, *2*, 586−593.
(22) Biel, B.; Blase, X.; Triozon, F.; Roche, S. *Phys. Rev. Lett.* **2009**, *102* (9), 096803−096806.
(23) Soler, J. M.; Artacho, E.; Gale, J. D.; García, A.; Junquera, J.; Ordejón, P.; Sánchez-Portal, D. *J. Phys.: Condens. Matter* **2002**, *14* (11), 2745−2779.
(24) Perdew, J. P.; Burke, K.; Ernzerhof, M. *Phys. Rev. Lett.* **1996**, *77* (18), 3865−3868.
(25) Perdew, J. P.; Ruzsinszky, A.; Csonka, G. I.; Vydrov, O. A.; Scuseria, G. E.; Constantin, L. A.; Zhou, X.; Burke, K. *Phys. Rev. Lett.* **2008**, *100* (13), 136406−136409.
(26) Troullier, N.; Martins, J.-L. *Phys. Rev. B* **1991**, *43* (3), 1993−2006.
(27) Artacho, E.; Sánchez-Portal, D.; Ordejón, P.; García, A.; Soler, J. M. *Phys. Status Solidi B* **1999**, *215* (1), 809−817.
(28) Soriano, D.; Fernández-Rossier, J. *Phys. Rev. B* **2012**, *85* (19), 195433−195441.
(29) Lambin, Ph.; Amara, H.; Ducastelle, F.; Henrard, L. *Phys. Rev. B* **2012**, *86* (4), 045448−045451.
(30) In the present orthogonal third nearest-neighbors π-π^* TB model, the parametrization of the N dopant consists in modifying both the onsite and the hopping terms as: $\delta\varepsilon_{p_z} = -4.60$ eV, $\delta\gamma_0^1 = +1.04$ eV, $\delta\gamma_0^2 = -0.03$ eV, $\delta\gamma_0^3 = +0.08$ eV.
(31) The band gap edges in Figure 2 are considered to be reached when $\rho(E) < 10^{-2}\,\mathrm{eV}^{-1}\,\mathrm{nm}^{-2}$.
(32) Pereira, V. M.; Lopes dos Santos, J. M. B.; Castro, A. H. Neto. *Phys. Rev. B* **2008**, *77* (11), 115109−115115.
(33) (a) Roche, S.; Mayou, D. *Phys. Rev. Lett.* **1997**, *79* (13), 2518−2521. (b) Lherbier, A.; Biel, B.; Niquet, Y. M.; Roche, S. *Phys. Rev. Lett.* **2008**, *100* (3), 036803−036806. (c) Leconte, N.; Lherbier, A.; Varchon, F.; Ordejón, P.; Roche, S.; Charlier, J.-C. *Phys. Rev. B* **2011**, *84* (23), 235420−235431.
(34) Leconte, N.; Soriano, D.; Roche, S.; Ordejón, P.; Charlier, J.-C.; Palacios, J. J. *ACS Nano* **2011**, *5* (5), 3987−3992.
(35) Joucken, F.; Tison, Y.; Lagoute, J.; Dumont, J.; Cabosart, D.; Zheng, B.; Repain, V.; Chacon, C.; Girard, Y.; Botello-Méndez, A. R.; Rousset, S.; Sporken, R.; Charlier, J.-C.; Henrard, L. *Phys. Rev. B (R)* **2012**, *85* (16), 161408−161412.
(36) Kim, K.; Choi, J.-Y.; Kim, T.; Cho, S.-H.; Chung, H.-J. *Nature* **2011**, *479* (7373), 338−344.
(37) Deng, X.; Wu, Y.; Dai, J.; Kang, D.; Zhang, D. *Phys. Lett. A* **2011**, *375* (44), 3890−3894.
(38) (a) Ci, L.; Song, L.; Jin, C.; Jariwala, D.; Wu, D.; Li, Y.; Srivastava, A.; Wang, Z. F.; Storr, K.; Balicas, L.; Liu, F.; Ajayan, P. M. *Nat. Mater.* **2010**, *9* (5), 430−435. (b) da Rocha Martins, J.; Chacham, H. *Phys. Rev. B* **2012**, *86* (7), 075421−075425.
(39) Marconcini, P.; Cresti, A.; Triozon, F.; Fiori, G.; Biel, B.; Niquet, Y. M.; Macucci, M.; Roche, S. *ACS Nano* **2012**, *6* (9), 7942−7947.